FISEVIER

Contents lists available at ScienceDirect

# Journal of Magnetism and Magnetic Materials

journal homepage: www.elsevier.com/locate/jmmm



#### Research articles

# Synthesis and characterization of iron oxide superparticles with various polymers



Shomit Mansur<sup>a</sup>, Anish Rai<sup>b</sup>, Robert A. Holler<sup>c</sup>, Tim Mewes<sup>b</sup>, Yuping Bao<sup>a,\*</sup>

- <sup>a</sup> Box 870203, Chemical and Biological Engineering, The University of Alabama, Tuscaloosa AL35487, United States
- <sup>b</sup> Box 870324, Department of Physics and Astronomy, The University of Alabama, Tuscaloosa AL35487, United States
- <sup>c</sup> Analytical Facility Center, The University of Alabama, Tuscaloosa AL35487, United States

#### ARTICLE INFO

Keywords: Iron oxide superparticles Solvothermal synthesis Polymer coating Magnetic separation

#### ABSTRACT

Iron oxide superparticles referring to a cluster of smaller nanoparticles have recently attracted much attention because of their enhanced magnetic moments but maintaining superparamagnetic behavior. In this study, iron oxide superparticles have been synthesized using a solvothermal method in the presence of six different polymers (e.g., sodium polyacrylate, pectin sodium alginate, chitosan oligosaccharides, polyethylene glycol, and polyvinylpyrrolidine). The functional group variation in these polymers affected their interactions with precursor iron ions, and subsequently influenced crystalline grain sizes within superparticles and their magnetic properties. These superparticles were extensively characterized by transmission electron microscopy, dynamic light scattering, x-ray diffraction, Fourier transform infrared spectroscopy, and vibrating sample magnetometry.

#### 1. Introduction

Iron oxide superparticles are defined as a cluster or assembly of smaller nanoparticles formed by controlled aggregation during or after synthesis [1]. Recently, superparticles have gained much interest due to their unique magnetic properties and applications in magnetic separation [2], targeted drug delivery [3], and magnetically responsive photonic crystals [4,5]. Because of the superparamagnetic limit of magnetic nanoparticles [6], magnetic iron oxide nanoparticles exhibit superparamagnetic to ferromagnetic transition around 25 nm at room temperature depending on the magnetic phases [6]. Above superparamagnetic limits, strong ferromagnetic interactions between nanoparticles lead to nanoparticle aggregation in solution, limiting their use in biological applications and magnetic separations. The formation of iron oxide superparticles (or nanoclusters) potentially overcomes this limitation by increasing magnetic moments for rapid magnetic response under a magnetic field gradient but maintaining superparamagnetic behavior [1].

In the past decade, several synthetic methods have been developed for the preparation of iron oxide superparticles by either clustering smaller nanoparticles during synthesis or assembly of nanoparticles after synthesis [1]. For example, ligand etching method produces magnetic superparticles by replacing the original capping molecules of

ligand-capped nanoparticles after synthesis with weakly bound ligands, which causes nanoparticle destabilization and subsequent aggregation [7]. The solvophobic interaction method involves micelle structure formation by dispersing hydrophobic ligand-coated nanoparticles in a surfactant aqueous solution, followed by an annealing process in the presence of capping molecules at elevated temperature (e.g., 80 °C) [8,9]. The solvothermal process generates superparticles in a single step by reacting reactants in a reducing solvent in a sealed hydrothermal reactor at high temperature (> 200 °C) [10-14]. And the polyol method involves injection of iron salts into a polyol solution at high temperature (> 200 °C) under basic conditions [4,15-17]. Among these methods, ligand etching and solvophobic interactions produce iron oxide superparticles by controlled assembly of uniform, already synthesized, ligand-capped nanoparticles (10-20 nm) into clusters under specific processing conditions. In contrast, iron oxide superparticles were synthesized in a single step for solvothermal process or polyol methods, where smaller nanoparticles first nucleated and grew in a supersaturated solution and then aggregated into larger clusters in a single step. Among all these methods, solvothermal method is very attractive because of its simplicity and scalability [14]. Compared to the polyol method involving hot base injection during reaction, the solvothermal method has less safety concern. In addition, as-synthesized superparticles are easily dispersed in aqueous solutions for

Abbreviations: PAA, sodium polyacrylate; PEG, polyethylene glycol; PVP, polyvinylpyrrolidine; TEM, transmission electron microscopy; DLS, dynamic light scattering; FTIR, Fourier transform infrared; XRD, x-ray diffraction; VSM, vibrating sample magnetometer; M-H, magnetization versus applied magnetic field

E-mail address: ybao@eng.ua.edu (Y. Bao).

<sup>\*</sup> Corresponding author.

various applications [14]. During solvothermal reactions, iron oxide superparticles were produced by reacting reagents (iron precursor, capping molecules, pH modifier, and reducing solvent) in a sealed, Teflon-lined stainless steel hydrothermal reactor at high temperatures [14]. Here, ethylene glycol is normally used as both a solvent and a reducing source. In addition, the sealed reactor also leads to pressurized heating. For the solvothermal method, the effects of specific reaction parameters on the superparticle formation were mainly focused on controlling grain size and size distribution of superparticles by adjusting the molar ratios of solvents and reactants [10]. Until now, only a few capping ligands have been studied, such as sodium citrate [14], polyacrylic acids [18], polyvinylpyrrolidine [10], and 5-sulfosalicylic acid [13]. In fact, the surface chemistry of the superparticles is critical for biological interfaces during applications. It is highly desirable to create iron oxide superparticles with various surface chemistry.

One of the most notable benefits of iron oxide superparticles is their use in magnetic separation or enrichment of biological entities [1], such as biomolecules [19-21] and organisms [2,22]. Individual iron oxide nanoparticles below the superparamagnetic limit have large surface areas but are insufficient to overcome drag forces in solution for efficient and rapid magnetic separation. Superparticles containing many smaller superparamagnetic nanoparticles have a higher total magnetic moment, which allows for efficient magnetic separation. We recently developed a new magnetic drug screening nanoplatform based on cell membrane encapsulated iron oxide nanoparticles [23], where cell membrane with functional transmembrane receptors were immobilized on iron oxide nanoparticles. The surface receptors act as "smart baits" for direct compound binding. The limitation of this drug screening platform was slow magnetic response because of the use of small superparamagnetic nanoparticles, and uncontrolled numbers of nanoparticle encapsulation. Cell-membrane encapsulated polymeric nanoparticles have been well studied for drug delivery and tumor targeting [24–28] and energy conversion [29]. Systematic studies using polymer nanoparticles and various cell types suggested a preferred nanoparticle core size in the range of 100-300 nm for effective cell membrane encapsulation [30,31]. In addition, negatively charged surfaces of polymer nanoparticles facilitated cell membrane coverage and positively charged surfaces formed aggregation of cell membrane fragments and nanoparticles [30,31]. Depending on the types of transmembrane receptors, the surface chemistry of nanoparticles may affect the states of the immobilized receptors, such as ion channels (open or close), because the surface coatings of the nanoparticles directly interface with the inner parts of the cell membranes. Therefore, preparation of superparamagnetic iron oxide nanoparticles in the size range of 100-300 nm with various surface chemistry will be desirable for further development of our newly developed magnetic drug screening plat-

In this paper, we successfully synthesized iron oxide superparticles with six different polymers, namely sodium polyacrylate (PAA), pectin, sodium alginate, chitosan, polyethylene glycol (PEG) and polyvinylpyrrolidine (PVP) using a solvothermal method. The effects of the polymers on the iron oxide superparticles were extensively characterized, including size and morphology by transmission electron microscopy (TEM), hydrodynamic size and zeta-potential by dynamic light scattering (DLS), surface chemistry by Fourier transform infrared (FTIR), crystal phase and grain size by x-ray diffraction (XRD), and magnetic properties by vibrating sample magnetometry (VSM) at room temperature.

#### 2. Materials and methods

# 2.1. Materials

All the chemical reagents were commercially purchased and used without further purification: ferric chloride (FeCl<sub>3</sub>, ACROS, 98%), sodium acetate (VWR, 99%), ethylene glycol (VWR, 99%), sodium

polyacrylate solution (Sigma Aldrich, 45% water, MW = 1200), sodium alginate (TCI, very low viscosity), polyethylene glycol (VWR, MW = 1500), polyvinylpyrrolidine (Alfa Aeser, MW = 58,000), chitosan oligosaccharides (TCI, 98%), pectin (Sigma Aldrich, MW = 72,000). Bis-tris (Amresco, ultrapure grade).

#### 2.2. Synthesis of iron oxide superparticles

The iron oxide superparticles were synthesized by first mixing reactants (FeCl $_3$ , sodium acetate, and polymer) in ethylene glycol under stirring. Then, the well-dissolved mixture was reacted for 12 h in a sealed, Teflon-lined, stainless steel hydrothermal reactor at 200 °C. For each polymer, the reaction condition was determined experimentally based on the superparticle formation, superparticle size (< 400 nm), and size distribution.

Specifically, the molar ratio of FeCl<sub>3</sub> to polymer and solvent volume were adjusted to achieve the following optimized reaction conditions: Sodium polyacrylate: FeCl<sub>3</sub> (0.8 mmol, 0.129 g) was dissolved in 30 mL of ethylene glycol, followed by the addition of PAA water solution (8 mmol, 0.52 g) and sodium acetate (35 mmol, 2.87 g). The mixture was stirred for three hours at room temperature to obtain a well-dispersed clear solution before transferring into a 100 mL hydrothermal reactor. Pectin: FeCl<sub>3</sub> (9 mmol, 1.46 g) was mixed with pectin (4.45 mmol and 0.864 g) and sodium acetate (35 mmol, 2.871 g) in 90 mL of ethylene glycol. The mixture was stirred for five hours at room temperature before transferring into a 300 mL hydrothermal reactor. PVP: FeCl<sub>3</sub> (0.8 mmol, 0.129 g) was dissolved in 30 mL of ethylene glycol, followed by the addition of PVP (8 mmol, 0.88 g) and sodium acetate (35 mmol, 2.871 g). The mixture was stirred for three hours at room temperature to obtain a well-dispersed clear solution before transferring into a 100 mL hydrothermal reactor. PEG: FeCl<sub>3</sub> (0.8 mmol, 0.129 g) was dissolved in 30 mL of ethylene glycol, followed by addition of PEG (8 mmol, 0.35 g) and sodium acetate (35 mmol, 2.871 g). The mixture was stirred for three hours at room temperature to obtain a well-dispersed clear solution before transferring into a 100 mL hydrothermal reactor. Chitosan Oligosaccharides: FeCl<sub>3</sub> (6.3 mmol, 1.022 g) was mixed with chitosan (2.1 mmol, 1.052 g) and sodium acetate (44 mmol, 3.6 g) in 120 mL of ethylene glycol. The mixture was stirred for five hours at room temperature to obtain a well-dispersed clear solution before transferring into a 300 mL hydrothermal reactor. Sodium Alginate: FeCl<sub>3</sub> (9 mmol, 1.46 g) was mixed with sodium alginate (3.6 mmol, 0.713 g) and sodium acetate (44 mmol, 2.871 g) in 90 mL of ethylene glycol. The mixture was stirred for five hours at room temperature to obtain a well-dispersed clear solution before transferring into a 300 mL hydrothermal reactor.

Polymers of other molecular weights were also tested where superparticles were either non-uniform or off the targeted size range. The effects of different molecular weights for each polymer was different. For PVP, lower molecular weight (e.g., mW = 8000) led to the formation of much smaller nanoparticles around 50 nm. In contrast, compared to low mW (1500) PEG presented in the manuscript, higher molecular weight PEG (mW = 4500 and 8000) led to the formation of interconnected smaller particles. As for the chitosan, due to the solubility issue of high molecular weights, oligomers produced the most satisfactory results.

After 12 h reaction at 200 °C, iron oxide superparticles were collected from the hydrothermal reactors and then washed three times using deionized water/ethanol (1:4 v/v). After drying under vacuum, the superparticles were weighed and re-dispersed in deionized water to prepare 1 mg/mL solution for TEM. The solution was further diluted five times in Bis-Tris buffer (20 mM, pH 7.2) for measuring DLS and zeta potential while carefully weighted dried powders were used for FTIR, XRD and magnetometry.

#### 2.3. Characterization of iron oxide superparticles

The size and morphology of iron oxide superparticles were examined under TEM (Hitachi 7860). The surface charges and dynamic sizes of these superparticles in buffer solution were measured using a Malvern (Malvern, UK) Zetasizer Nano series dynamic light scattering instrument. The FTIR spectra were collected on a JASCO 4100 spectrometer, equipped with an attenuated total reflectance (ATR) cell by accumulation of 4 scans, with a resolution of 2 cm $^{-1}$ . The crystal structures of the superparticles in powder form were studied on a Bruker AXSD8 Advanced x-ray diffractometer (XRD) using a Co source (K $\alpha$ ,  $\lambda=1.79$ Å). The magnetic moment versus applied magnetic field (M-H) curves of these superparticles were recorded by a DMS vibrating sample magnetometer (VSM) at room temperature.

#### 3. Results and discussion

Iron oxide superparticles were successfully prepared in the presence of six different polymers using a solvothermal method. Compared to previous studies on controlling particle sizes by the ratios of solvents and reactants [10,12,14], here, the focus of our studies was to investigate polymer effects on the formation and properties of iron oxide superparticles. During the synthetic process, for each polymer, the ratios of precursor iron ion to polymer and solvent volume were adjusted for superparticle formation. The selected polymers, their structures, and properties are shown in Table 1, where the polymer variation contains functional groups and charged properties.

The types and numbers of functional groups and their interactions with precursor iron ions are important as nucleation sites for primary nanoparticle formation and growth. In addition, the binding affinity of polymers on iron oxide surfaces directly affects the aggregation process for the superparticle formation. Among these six polymers, sodium polyacrylate (PAA) has only carboxylic groups with a pKa around 4.5, leading to negatively charged surfaces at neutral pH. Pectin and alginate have very similar structures, both of which belong to polyuronates, but they interact with multivalent ions and other molecules differently [32,33]. Therefore, these two polymers may interact with the iron ion precursor differently. In addition to carboxylic groups, the large amount of hydroxyl groups from the sugar rings will affect the nucleation and growth of superparticles. Chitosan is a type of modified sugar molecules, and chitosan oligosaccharides are completely deacetylated with free amine groups. The pKa of the amine groups is around 6.5, which allows for tailoring the surface charges of chitosan around neutral pH to either positively charged (pH < 6.5) or negatively charged (pH > 7). Compared to these charged polymers, PEG and PVP are not charged. PEG molecules only contain a single hydroxyl group and ether groups, which are thought to be nonionic. However, the high electronegativity of oxygen makes PEG molecules highly hydrophilic, and attracts positively charged iron ions, serving as nucleation centers. PVP consists of a C=O group and a nitrogen (N) inside the ring, where iron ions link to the C=O groups while the negative counter ions interact with the slightly positively charged nitrogen. These polymers are expected to affect the superparticle formation greatly because of their different properties.

Fig. 1 shows the representative TEM images of as-synthesized iron oxide superparticles prepared using PAA, pectin, alginate, chitosan, PEG, and PVP from typical reactions. Despite a similar reaction process was used and all the superparticles were nearly spherical, the size and size distribution varied among these different surface coatings. For instance, about 150-200 nm of superparticles were synthesized using PAA, pectin, alginate, and PVP (Fig. 1A-C), but the superparticle sizes were much larger in the presence of PEG and chitosan (350-400 nm) (Fig. 1D and E). The formation of iron oxide superparticles suggested that all six polymers could nucleate and protect the primary iron oxide nanoparticles during the hydrothermal reaction. However, the presence of carboxylic groups were important for controlled growth due to the strong interactions between carboxylic groups and iron ions. In contrast, the superparticles formed in the presence of PEG and PVP showed uneven contrasts across particles on TEM images and cavities were observed in some of the superparticles (Fig. 1E and F), likely because the functional groups on these polymers did not allow effective interactions of the small nanoparticles in three dimensional. The superparticles formed using chitosan were much larger, likely because the amine groups could not effectively control the growth of the nanoparticles.

The hydrodynamic sizes of the superparticles synthesized with different polymers were measured in Bis-tris buffer at pH 7.2. Here, Bistris buffer was used for several reasons. First, the physiological pH falls within the useful pH range of the Bis-tris buffer (5.8-7.2); second, the buffer does not contain as much salts as in phosphate buffer saline, where salts have great effects on charged polymers; finally, the lack of the carboxylic and primary amine groups in Bis-tris avoids ionic interaction effects on polymer-coated superparticles. PAA-, pectin-, alginate-, and PVP-coated superparticles were around 180 nm, 250 nm, 210 nm, and 200 nm respectively (Fig. 2), which were in agreement with sizes from TEM. This size consistency suggested that those four polymers could effectively protect iron oxide superparticles. In contrast, the superparticles synthesized with PEG and chitosan molecules showed much broader peaks, suggesting PEG molecules may not effectively protect superparticles from aggregation in solution. The larger size of superparticles synthesized with chitosan has possibly resulted from the interactions between particles, as seen the dark background on the TEM image. At pH 7.2, the amine groups are deprotonated, leading to uncharged but polar amine groups. The lack of repulsion from the positively charged amines likely caused strong interactions between particles and a subsequent large hydrodynamic size.

The zeta-potential value of a colloidal solution indicates its stability with the zeta potential of a stable colloidal solution being higher than 30 mV or smaller than -30 mV [34]. The zeta potentials of all superparticle solutions except for PVP-coated superparticles were lower than -30 mV (-36 mV for PAA-coated, -40 mV for pectin-coated, -38 mV for PEG-coated, and -32 mV for chitosan-coated). The negatively charged surfaces for superparticles synthesized from PAA, pectin and alginate can be easily explained by the ionized -COO<sup>-</sup> groups. The pKa of chitosan is around 6.5, the amine groups will be deprotonated (-NH<sub>2</sub>) at pH 7.2, the measuring condition. The negative charges likely resulted from the high electronegativity of the large number of hydroxyl groups. Similar negatively charged surfaces

 Table 1

 Polymers used in iron oxide superparticle synthesis.

Polymers	Sodium Polyacrylate (PAA)	Pectin	Sodium Alginate	Chitosan	Polyethylene glycol (PEG)	Polyvinyl pyrrolidine
Structure	O ONA	HOOC MeOOC O	$\begin{array}{c} OH \\ OO $	OH OHO NH <sub>2</sub> n=15	$H = \begin{pmatrix} 0 & 1 \\ 0 & 1 \end{pmatrix}$	H H
Properties	pKa = 4.5 mW = 1200	pKa = 3.0-3.5 mW = 72,000	pKa = 1.5-3.5 mW = N/A	pKa = 6.5 mw≤3000		pKa = 4.2 mW = 58,000

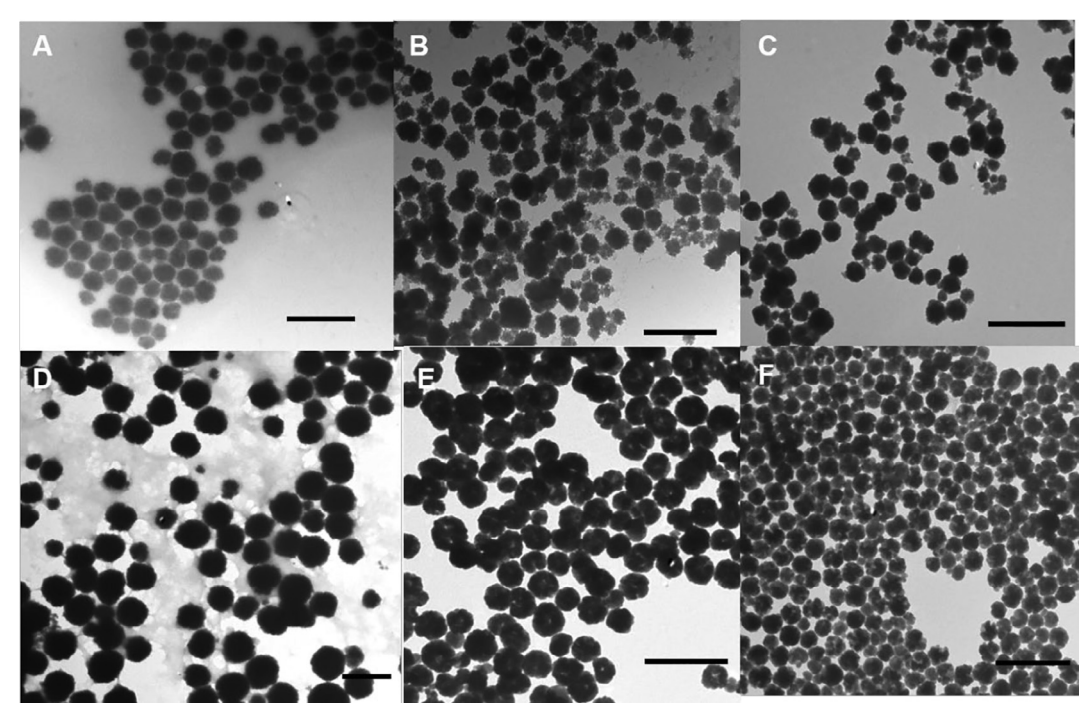


Fig. 1. Representative TEM images of iron oxide superparticles prepared using (A) PAA, (B) pectin (C) sodium alginate, (D) chitosan, (E) PEG and (F) PVP. Scale bar: 500 nm.

 $(-38\,$  mV) for PEG-coated superparticles were also observed. No charged groups are present in PVP molecules and the functional groups were likely coordinated with iron oxide surfaces [12], leading to a larger zeta-potential of -10 mV, indicating a nascent instability for this colloidal solution.

The presence of the polymers on superparticle surface were further confirmed with FTIR spectra (Fig. 3). The FTIR spectrum of PAA-coated superparticles showed the typical asymmetric (1555 cm<sup>-1)</sup> and symmetric (1403 cm<sup>-1)</sup> stretching of the carboxylate (COO<sup>-</sup>) groups [35]. The peak at 1042 cm<sup>-1</sup> was related to C–O stretching while the broad low intensity peak at 2864 cm<sup>-1</sup> and 888 cm<sup>-1</sup> corresponded to the C–H stretching and bending. Similar to PAA-coated superparticles, the FTIR spectrum of pectin-coated superparticles also exhibited the symmetric and asymmetric stretching of the COO<sup>-</sup> groups at 1621 and 1384 cm<sup>-1</sup> and C–O stretching at 1043 cm<sup>-1</sup> [36,37]. Additional, a strong O–H stretching band was observed around 3353 cm<sup>-1</sup>. Because of the similar structures of pectin and alginate, the FTIR spectra of these two samples were very similar with symmetric and asymmetric stretching of COO<sup>-</sup> groups at 1574 and 1393 cm<sup>-1</sup>, C–O stretching at

1042 cm<sup>-1</sup> [38,39] and a strong O-H stretching band around 3236 cm<sup>-1</sup>. For chitosan-coated superparticles, the FTIR spectrum showed several characteristic bands, overlapping O-H and N-H stretching band around 3300 cm<sup>-1</sup>, C-H stretching at 2931 cm<sup>-1</sup>, N-H bend at 1604 cm $^{-1}$ , and C-O stretch at 1043 cm $^{-1}$  [40,41]. The sharp peak at 1379 was likely related to O-H bending. The FTIR spectra of PEG-coated superparticles only showed a broad weak band around at 3200-3500 cm<sup>-1</sup> likely related to intermolecular bonded O-H stretching. However, the ether stretching band (C-O-C) at  $1045~\mathrm{cm}^{-1}$  was clearly observed. The band at 1410 cm corresponded to O-H bending. Similarly, C-H stretching at 2857 cm<sup>-1</sup> and C-H outof-plane bending at 879 cm<sup>-1</sup> were detected [42]. The band at 1589 cm<sup>-1</sup> can be attributed to asymmetric C-O stretching [43]. For PVP-coated superparticles, the FTIR spectrum showed characteristic C=O and C-N stretching at 1555 cm<sup>-1</sup> and 1375 cm<sup>-1</sup> respectively [44]. Similarly, the bands at 2916 cm<sup>-1</sup> and 882 cm<sup>-1</sup> corresponded to C-H stretching and C-H out-of-plane bending. The band at 1026 cm<sup>-1</sup> is likely related to C-N stretching as well. These FTIR spectra suggested that all the polymers were on the surface of the superparticles or in-

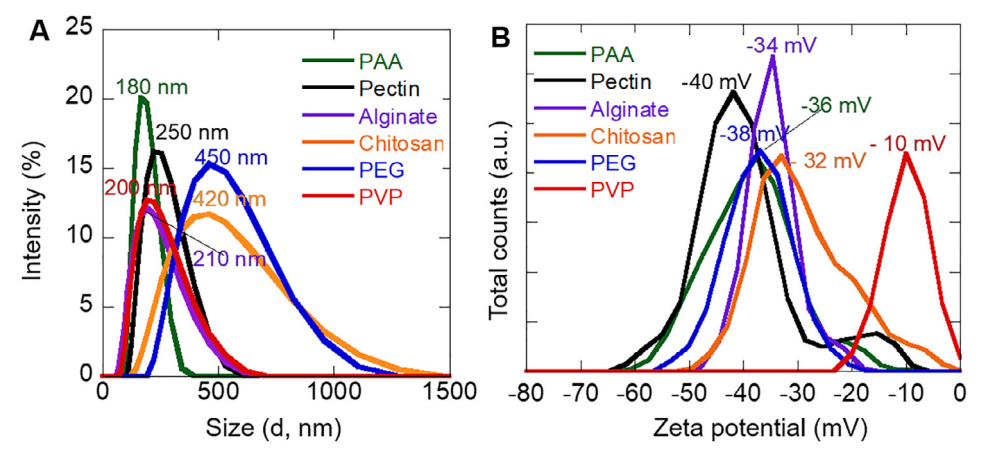


Fig. 2. Iron oxide superparticles in Bis-tris buffer at pH 7.2: (A) DLS plots, and (B) zeta potential plots.

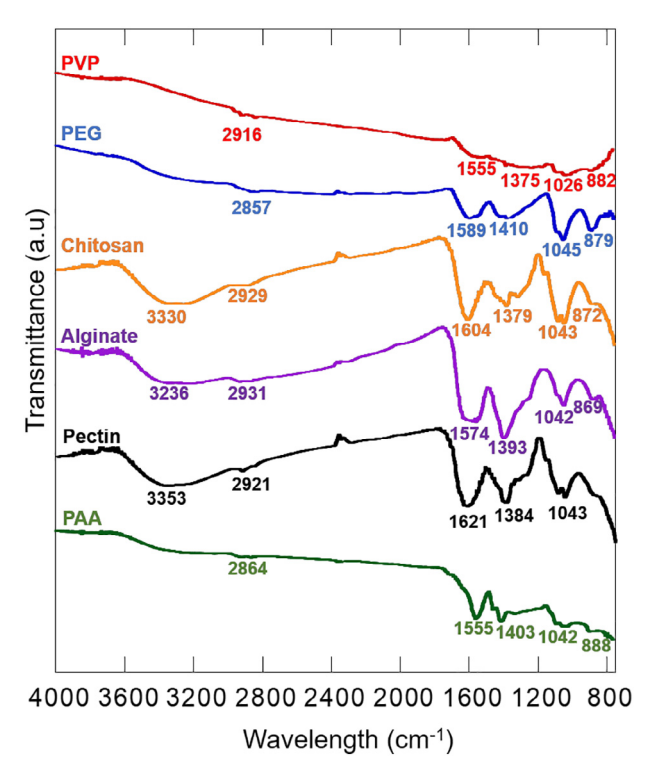


Fig. 3. FTIR spectra of iron oxide superparticles synthesized with PAA, pectin, alginate, chitosan, PEG, and PVP.

between of the primary nanoparticles.

The crystal phases of the polymer-coated iron oxide superparticles were studied by XRD and Fig. 4 shows the XRD patterns collected on powder samples. The major peaks in all six samples showed the same peak positions, all of which matched well with the standard crystal phase of magnetite. These diffraction peaks can be readily indexed as (200), (311), (400), (422), (511), and (440) planes. The diffraction peaks of (620), (533), and (444) planes were clearly observed for

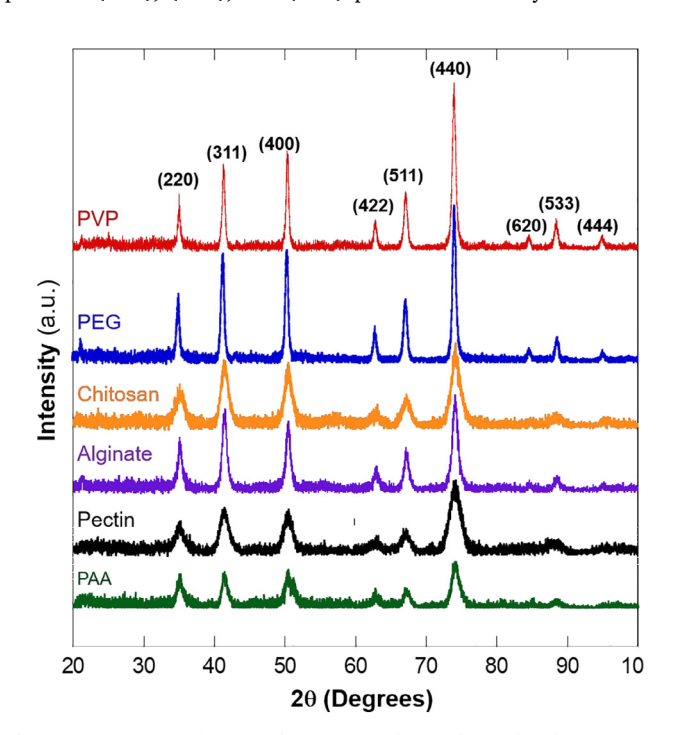


Fig. 4. XRD patterns of iron oxide superparticles synthesized with PAA, pectin, alginate, chitosan, PEG and PVP.

**Table 2**Grain sizes of the samples estimated based XRD (311) and (440) peaks and comparison with properties from TEM and DLS.

Sample	Grain size (nm) (311)	Grain size (nm) (440)	TEM size (nm)	DLS size (nm)	Zeta potential (mV)
PAA	7	19	160	180	- 36
Pectin	6	9	150	250	-40
Alginate	12	15	150	210	-34
Chitosan	7	11	320	420	-32
PEG	18	23	230	450	-38
PVP	22	29	180	200	-10

PEG- and PVP-coated superparticles, but which were significantly broadened for other samples. In addition, the peaks in PEG and PVP coated samples were much sharper, indicating larger grain sizes.

The crystallite grain sizes of each sample were estimated by Scherrer's equation using two high intensity peaks (311), and (440). The estimated grain sizes varied depending on the peak used for estimation, likely due to certain crystal orientation when preparing the samples. The estimated grain sizes for pectin, alginate, chitosan, PEG and PVP coated superparticles were similar using (311) or (440) peak. However, the estimated sizes for PAA-coated sample using these two peaks were much different (7 nm versus 19 nm). This observation was consistent with the relative low intensity and broadening of the (311) peak for PAA-coated superparticles (Fig. 4). The grain size estimation suggested that the polymers directly influenced superparticle formation during synthesis, including overall size and gain sizes. A summary of the estimated grain sizes is shown in Table 2. The much smaller grain sizes in all samples compared to the sizes measured from TEM and DLS suggested that these superparticles indeed composed of many smaller crystalline nanoparticles. The differences in the sizes based on TEM and hydrodynamic sizes from DLS were due to the surface capping polymers and their ionization states.

Fig. 5 shows the magnetization versus applied magnetic field (M-H) curves of iron oxide superparticles synthesized using PAA, pectin, alginate, chitosan, PEG and PVP polymers measured by VSM at room temperature. The insert of each curve was plotted in a lower magnetic field range ( $-1000 \sim 1000$  Oe) to observe the presence of coercivity. The saturation magnetization was calculated to be 36.0 emu/g for PAAcoated superparticles, 42.3 emu/g for pectin-coated superparticles, 60.1 emu/g for alginate-coated superparticles, 36.4 emu/g for chitosancoated superparticles, 67.7 emu/g for PEG-coated superparticles and 77.2 emu/g for PVP-coated superparticles. These saturation magnetization values were significantly smaller than the value of bulk magnetite (92 emu/g), because the saturation magnetization was calculated based on the sample mass including the superparticles and polymers. The superparticles synthesized with PAA, pectin and chitosan all exhibited superparamagnetic behaviors (Fig. 5A, B, and D), consistent with their estimated small grain sizes from XRD. In contrast, the M-H curves of PEG and PVP coated superparticles showed open hysteresis loops with observed coercivity of 45.0 Oe and 75.5 Oe respectively (Fig. 5E and F). These observation are also consistent with the calculated larger grain sizes of PEG and PVP-coated superparticles, which are close to range of the superparamagnetic limit of iron oxide nanoparticles. An open hysteresis loop with a coercivity of 30.5 Oe was also observed for the M-H curve of alginate-coated superparticles, which was not expected for the estimated grain sizes based on XRD, possibly due to the presence of some aggregated superparticles during cleaning and sample drying. The values of the saturation magnetization and coercivity for all six samples are summarize in Table 3. The magnetic measurement indicated the polymers can be used to tune the grain sizes of the superparticles and their subsequent magnetic properties. Because of the superparamagnetic preferences, these magnetic measurements also suggested that superparticles synthesized with PAA, pectin and chitosan are more preferable for magnetic separation.

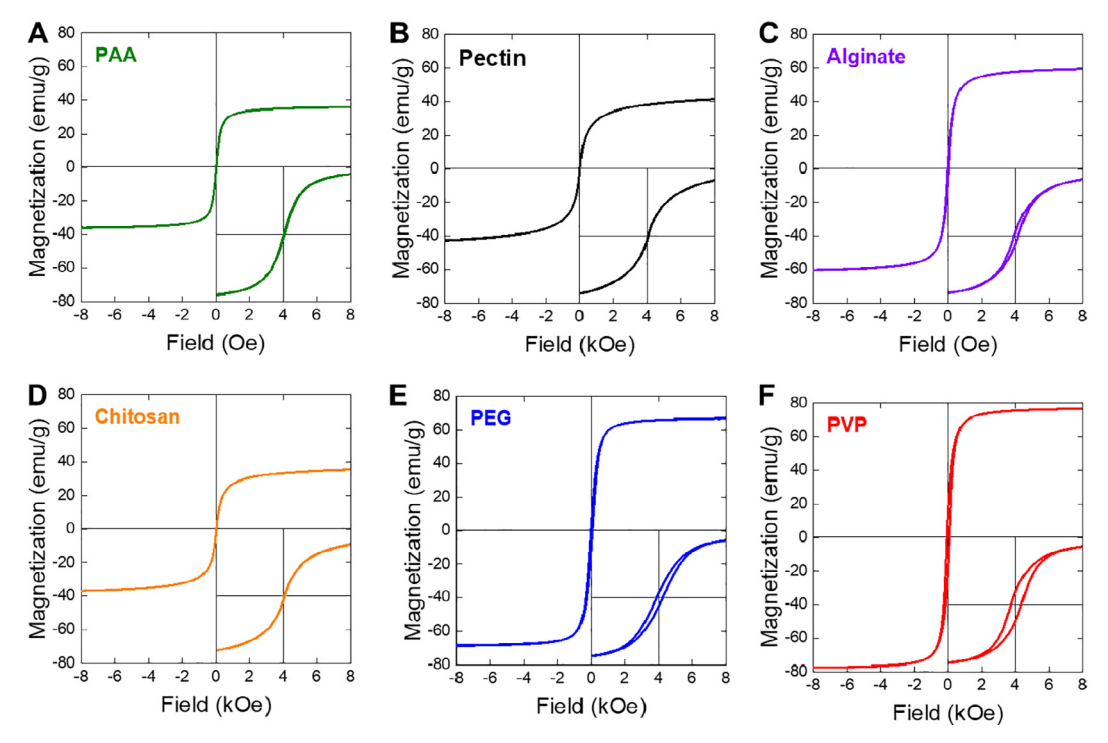


Fig. 5. Room-temperature M-H curves with close views (-1000 to 1000 Oe, insets) of iron oxide superparticles synthesized with: (A) PAA, (B) pectin, (C) alginate, (D) chitosan, (E) PEG, and (F) PVP.

Table 3

Magnetic parameters of polymer-coated iron oxide superparticles

magnetic parameters of polymer coated from onace superparticles.						
Sample	Magnetization (M <sub>s</sub> ) (emu/g)	Corecivity (H <sub>c</sub> ) (Oe)	Remanence (M <sub>r</sub> ) (emu/g)			
PAA	36	0	0			
Pectin	42.3	0	0			
Alginate	60.1	30.5	5.7			
Chitosan	36.4	0	0			
PEG	67.7	45.0	6.7			
PVP	77.2	75.6	17.5			

#### 4. Conclusion

In summary, we have successfully synthesized iron oxide superparticles using six different polymers, such as PAA, pectin, alginate, chitosan, PEG and PVP. Even though these polymers have different functional groups (-COOH, -OH, -NH<sub>2</sub>, or -C=O), they were all able to nucleate and direct the growth of iron oxide superparticles in hydrothermal reactors at high temperature. The presence of these polymers within superparticles were confirmed by FTIR. Regardless of the polymer types, all six polymers led to the formation of iron oxide superparticles in magnetite phase. However, the differences in binding affinity of the functional groups on different polymers resulted in grain size variation determined by XRD. Among these six polymers, PEG and PVP provided the least control of growth, leading to larger grain sizes. Consistent with the estimated grain sizes, the superparticles with smaller grain sizes (e.g., PAA, pectin and chitosan coated samples) showed typical superparamagnetic behaviors at room temperature. In contrast, PEG and PVP-coated superparticles showed ferromagnetic behaviors with non-zero coercivity and remanence. Our studies will greatly benefit magnetic separation which require different surface chemistry for immobilization.

## CRediT authorship contribution statement

Shomit Mansur: Investigation, Data curation, Writing - original

draft. **Anish Rai:** Data curation, Visualization. **Robert A. Holler:** Data curation. **Tim Mewes:** Validation, Writing - review & editing. **Yuping Bao:** Project administration, Funding acquisition, Writing - review & editing.

#### **Declaration of Competing Interest**

The authors declare that they have no known competing financial interests or personal relationships that could have appeared to influence the work reported in this paper.

#### Acknowledgments

This work was supported by NSF-CBET 1915873 and Merrymac-McKcinley Foundation Award. Y.B acknowledges Alabama Life Research Institute for seed funding support and Center for Clinical and Translational Science Therapeutic Advancement Initiative award from University of Alabama at Birmingham. A. R. would like to acknowledge support by DARPA TEE Award No. D18AP00011.

### Appendix A. Supplementary data

Supplementary data to this article can be found online at https://doi.org/10.1016/j.jmmm.2020.167265.

#### References

- A.J. Antone, Z. Sun, Y. Bao, Preparation and application of iron oxide nanoclusters, Magnetochemistry 5 (2019) 16.
- [2] Y.T. Kim, K.H. Kim, E.S. Kang, G. Jo, S.Y. Ahn, S.H. Park, S.I. Kim, S. Mun, K. Baek, B. Kim, K. Lee, W.S. Yun, Y.H. Kim, Synergistic effect of detection and separation for pathogen using magnetic clusters, Bioconjugate Chem. 27 (2016) 59–65.
- [3] B. Luo, S. Xu, A. Luo, W.R. Wang, S.L. Wang, J. Guo, Y. Lin, D.Y. Zhao, C.C. Wang, Mesoporous biocompatible and acid-degradable magnetic colloidal nanocrystal clusters with sustainable stability and high hydrophobic drug loading capacity, Acs Nano 5 (2011) 1428–1435.
- [4] J. Ge, Y. Hu, Y. Yin, Highly tunable superparamagnetic colloidal photonic crystals, Angew. Chem. Int. Ed. 46 (2007) 7428–7431.
- 5] P. Yang, H. Li, S. Zhang, L. Chen, H. Zhou, R. Tang, T. Zhou, F. Bao, Q. Zhang, L. He,

- X. Zhang, Gram-scale synthesis of superparamagnetic Fe3O4 nanocrystal clusters with long-term charge stability for highly stable magnetically responsive photonic crystals, Nanoscale 8 (2016) 19036–19042.
- [6] Y. Bao, T. Wen, A.C.S. Samia, A. Khandhar, K.M. Krishnan, Magnetic nanoparticles material engineering and emerging applications in lithography and biomedicine, J. Mater. Sci. 50 (2015) 1–44.
- [7] J. Fu, L. He, W. Xu, J. Zhuang, X. Yang, X. Zhang, M. Wu, Y. Yin, Formation of colloidal nanocrystal clusters of iron oxide by controlled ligand stripping, ChemComm 52 (2016) 128–131.
- [8] J. Zhuang, H. Wu, Y. Yang, Y. Cao, Controlling colloidal superparticle growth through solvophobic interactions, Angew. Chem. Int. Ed. 47 (2008) 2208–2212.
- [9] J. Zhuang, H. Wu, Y. Yang, Y. Cao, Supercrystalline colloidal particles from artificial atoms, J. Am. Chem. Soc. 129 (2007) 14166–14167.
- [10] S. Xuan, Y.X.J. Wang, J.C. Yu, K.C.F. Leung, Tuning the grain size and particle size of superparamagnetic Fe3O4 microparticles, Chem. Mater. 21 (2009) 5079–5087.
- [11] J. Gao, X. Ran, C. Shi, H. Cheng, T. Cheng, Y. Su, One-step solvothermal synthesis of highly water-soluble, negatively charged superparamagnetic Fe3O4 colloidal nanocrystal clusters, Nanoscale 5 (2013) 7026–7033.
- [12] S. Li, T. Zhang, R. Tang, H. Qiu, C. Wang, Z. Zhou, Solvothermal synthesis and characterization of monodisperse superparamagnetic iron oxide nanoparticles, J. Magn. Magn. Mater. 379 (2015) 226–231.
- [13] W. Wang, B. Tang, S. Wu, Z. Gao, B. Ju, X. Teng, S. Zhang, Controllable 5-sulfo-salicylic acid assisted solvothermal synthesis of monodispersed superparamagnetic Fe3O4 nanoclusters with tunable size, J. Magn. Magn. Mater. 423 (2017) 111–117.
- [14] J. Kim, V.T. Tran, S. Oh, C.S. Kim, J.C. Hong, S. Kim, Y.S. Joo, S. Mun, M.H. Kim, J.W. Jung, J. Lee, Y.S. Kang, J.W. Koo, Scalable solvothermal synthesis of superparamagnetic Fe3O4 nanoclusters for bioseparation and theragnostic probes, Acs Appl. Mater. Interfaces 10 (2018) 41935–41946.
- [15] J. Ge, Y. Hu, M. Biasini, C. Dong, J. Guo, W.P. Beyermann, Y. Yin, One-step synthesis of highly water-soluble magnetite colloidal nanocrystals, Chem. Eur. J. 13 (2007) 7153–7161.
- [16] J. Ge, Y. Hu, M. Biasini, W.P. Beyermann, Y. Yin, Superparamagnetic magnetite colloidal nanocrystal clusters, Angew. Chem. Int. Ed. 46 (2007) 4342–4345.
- [17] Z. Lu, Y. Yin, Colloidal nanoparticle clusters: functional materials by design, Chem. Soc. Rev. 41 (2012) 6874–6887.
- [18] J. Liang, H. Ma, W. Luo, S. Wang, Synthesis of magnetite submicrospheres with tunable size and superparamagnetism by a facile polyol process, Mater. Chem. Phys. 139 (2013) 383–388.
- [19] J. Zhang, M. Zhu, Y. Yang, J. Cao, F. Shi, Extraction of genomic DNA via superparamagnetic Fe3O4 magnetic colloidal nanocrystal clusters, J. Nanosci. Nanotechnol. 18 (2018) 8105–8110.
- [20] S. Meerod, N. Deepuppha, B. Rutnakornpituk, M. Rutnakornpituk, Reusable magnetic nanocluster coated with poly(acrylic acid) and its adsorption with an antibody and an antigen, J. Appl. Polym. Sci. 135 (2016) 46160.
- [21] X. Long, J. Li, D. Sheng, H. Lian, Low-cost iron oxide magnetic nanoclusters affinity probe for the enrichment of endogenous phosphopeptides in human saliva, Rsc Adv. 6 (2016) 96212.
- [22] C. Wen, Y. Jiang, X. Li, M. Tang, L. Wu, J. Hu, D. Pang, J. Zeng, Efficient enrichment and analyses of bacteria at ultralow concentration with quick-response magnetic nanospheres, Acs Appl. Mater. Interfaces 9 (2017) 9416–9425.
- [23] J. Sherwood, J. Sowell, N. Beyer, J. Irvin, C. Stephen, A.J. Antone, Y. Bao, L.M. Ciesla, Cell-membrane coated iron oxide nanoparticles for isolation and specific identification of drug leads from complex matrices, Nanoscale 11 (2019) 6352–6359.
- [24] P. Guo, J. Huang, Y. Zhao, C.R. Martin, R.N. Zare, M.A. Moses, Nanomaterial preparation by extrusion through nanoporous membranes, Small 14 (2018) 1703493.
- [25] A. Narain, S. Asawa, V. Chhabria, Y. Patil-Sen, Cell membrane coated nanoparticles: next-generation therapeutics, Nanomedicine 12 (2017) 2677–2692.

- [26] A.V. Kroll, R.H. Fang, L. Zhang, Biointerfacing and applications of cell membranecoated nanoparticles, Bioconjugate Chem. 28 (2017) 23–32.
- [27] W. Gao, L. Zhang, Coating nanoparticles with cell membranes for targeted drug delivery, J. Drug Targeting 23 (7–8) (2015) 619–626.
- [28] C.-M.-J. Hu, R.H. Fang, K.-C. Wang, B.T. Luk, S. Thamphiwatana, D. Dehaini, N. Phu, P. Angsantikul, C.H. Wen, A.V. Kroll, C. Carpenter, M. Ramesh, V. Qu, S.H. Patel, J. Zhu, W. Shi, F.M. Hofman, T.C. Chen, W. Gao, K. Zhang, S. Chien, L. Zhang, Nanoparticle biointerfacing by platelet membrane cloaking, Nature 526 (2015) 118–121.
- [29] Z. Chen, H. Zhang, P. Guo, J. Zhang, G. Tira, Y.J. Kim, Y.M.A. Wu, Y. Liu, J. Wen, T. Rajh, J. Niklas, O.G. Poluektov, P.D. Laible, E.A. Rozhkova, Semi-artificial photosynthetic CO<sub>2</sub> reduction through purple membrane re-engineering with semiconductor, J. Am. Chem. Soc. 141 (2019) 11811–11815.
- [30] B.T. Luk, C.M.J. Hu, R.N.H. Fang, D. Dehaini, C. Carpenter, W. Gao, L. Zhang, Interfacial interactions between natural RBC membranes and synthetic polymeric nanoparticles, Nanoscale 6 (2014) 2730–2737.
- [31] H.S. Jang, The diverse range of possible cell membrane interactions with substrates: drug delivery, interfaces and mobility, Molecules 22 (2017) 2197.
- [32] B. Zhang, B. Hu, M. Nakauma, T. Funami, K. Nishinari, K.I. Draget, G.O. Phillips, Y. Fang, Modulation of calcium-induced gelation of pectin by oligoguluronate as compared to alginate, Food Res. Int. 116 (2019) 232–240.
- [33] C.K. Siew, P.A. Williams, N.W.G. Young, New insights into the mechanism of gelation of alginate and pectin: charge annihilation and reversal mechanism, Biomacromolecules 6 (2005) 963–969.
- [34] E. Taboada, E. Rodriguez, A. Roig, J. Oro, A. Roch, R.N. Muller, Relaxometric and magnetic characterization of ultrasmall iron oxide nanoparticles with high magnetization. Evaluation as potential T-1 magnetic resonance imaging contrast agents for molecular imaging, Langmuir 23 (2007) 4583—4588.
- [35] Y. Xu, Y. Qin, S. Palchoudhury, Y. Bao, Water-soluble iron oxide nanoparticles with high stability and selective surface functionality, Langmuir 27 (2011) 8990–8997.
- [36] F. Ghibaudo, E. Gerbino, G.J. Copello, V.C.D. Orto, A. Gomez-Zavaglia, Pectin-decorated magnetite nanoparticles as both iron delivery systems and protective matrices for probiotic bacteria, Colloids Surf. B 180 (2019) 193–201.
- [37] F.J. Ngenefeme, N.J. Eko, Y.D. Mbom, N.D. Tantoh, K.M. Rui, A one pot green synthesis and characterisation of iron oxide-pectin hybrid nanocomposite, Open J. Compos. Mater. 3 (2013) 30–37.
- [38] H. Ma, X. Qi, Y. Maitani, T. Nagai, Preparation and characterization of superparamagnetic iron oxide nanoparticles stabilized by alginate, Int. J. Pharm. 333 (2007) 177–186.
- [39] J. Castello, M. Gallardo, M.A. Busquets, J. Estelrich, Chitosan (or alginate)-coated iron oxide nanoparticles: a comparative study, Colloids Surf. A 468 (2015) 151–158.
- [40] A.V. Samrot, N. Shobana, P.D. Sruthi, C.S. Sahithya, Utilization of chitosan-coated superparamagnetic iron oxide nanoparticles for chromium removal, Appl. Water Sci. 8 (2018) 192.
- [41] P.I.P. Soares, D. Machado, C. Laia, L.C.J. Pereira, J.T. Coutinho, I.M.M. Ferreira, C.M.M. Novo, J.P. Borges, Thermal and magnetic properties of chitosan-iron oxide nanoparticles, Carbohydr. Polym. 149 (2016) 382–390.
- [42] A.K. Gupta, S. Wells, Surface-modified superparamagnetic nanoparticles for drug delivery: preparation, characterization, and cytotoxicity studies, IEEE Trans. Nanobiosci. 3 (2004) 66–73.
- [43] S. Boonjamnian, T. Trakulsujaritchok, K. Srisook, V.P. Hoven, P.N. Nongkhai, Biocompatible zwitterionic copolymer-stabilized magnetite nanoparticles: a simple one-pot synthesis, antifouling properties and biomagnetic separation, Rsc Adv. 8 (2018) 37077–37084.
- [44] R.K. Gangwar, V.A. Dhumale, D. Kumari, U.T. Nakate, S.W. Gosavi, R.B. Sharma, S.N. Kale, S. Datar, Conjugation of curcumin with PVP capped gold nanoparticles for improving bioavailability, Mat. Sci. Eng. C 32 (2012) 2659–2663.